HOKKAIDO UNIVERSITY

Title	First two-micron imaging polarimetry of beta Pictoris
Author(s)	Tamura, Motohide; Fukagawa, Misato; Kimura, Hiroshi et al.
Citation	The astrophysical journal. Part 1, 641(2), 1172-1177 https://doi.org/10.1086/500575
Issue Date	2006-04-20
Doc URL	https://hdl.handle.net/2115/8925
Rights	C2006 The American Astronomical Society. The astrophysical journal. Part 1. vol. 641 p. 1172-1177
Type	journal article
File Information	63815.web.pdf

Hokkaido University Collection of Scholarly and Academic Papers : HUSCAP

The Astrophysical Journal, 641:1172–1177, 2006 April 20
© 2006. The American Astronomical Society. All rights reserved. Printed in U.S.A.

FIRST TWO-MICRON IMAGING POLARIMETRY OF β PICTORIS

Motohide Tamura,[1,2] Misato Fukagawa,[1,3,4] Hiroshi Kimura,[5] Tetsuo Yamamoto,[5] Hiroshi Suto,[1] and Lyu Abe[1]

Received 2005 October 5; accepted 2005 December 8

ABSTRACT

High-resolution *K*-band imaging polarimetry of the β Pic dust disk has been conducted with adaptive optics and a coronagraph using the Subaru 8.2 m telescope. Polarization of $\sim$10% is detected out to $r \sim 120$ AU with a centrosymmetric vector pattern around the central star, confirming that the disk is seen as an infrared reflection nebula. We have modeled our near-infrared and previous optical polarization results in terms of dust scattering in the disk and have found that both the degrees of polarization and the radial intensity profiles are well reproduced. We argue that the observed characteristics of the disk dust are consistent with the presence of ice-filled fluffy aggregates consisting of submicron grains in the β Pic system. There is a gap around 100 AU in both the intensity and polarization profiles, which suggests a paucity of planetesimals in this region. The radial intensity profile also shows ripple-like structures, which are indicative of the presence of multiple planetesimal belts, as in the case of the M-type Vega-like star AU Mic.

Subject headings: circumstellar matter — infrared: stars — planetary systems: protoplanetary disks — polarization — stars: individual (β Pic)

1. INTRODUCTION

The A5 V star β Pic (R.A. = $5^h47^m17^s.08$, decl. = $-51°3'59''.5$ (J2000.0); $V = 3.85$, $K = 3.53$, $d = 19.28$ pc, age $\sim$20 Myr) was among the first main-sequence stars for which significant excess infrared emission was detected by the *Infrared Astronomical Satellite* (*IRAS*) (Aumann et al. [1984]; see Crifo et al. [1997] for distance and Barrado y Navascués et al. [1999] for age). Subsequent observations have revealed that the infrared emission is due to the presence of a dusty disk around the star. Because the faint circumstellar disk lies near the very bright central star, various techniques for achieving a high contrast have been employed to directly observe the circumstellar structure. The first successful observations were made with an optical CCD coronagraph, which clearly detected scattered light from a nearly edge-on dust disk (Smith & Terrile 1984), then followed by antiblooming CCD imaging, new optical coronagraph imaging, near-infrared adaptive optics (AO) imaging, and *Hubble Space Telescope* (*HST*) optical imaging (Lecavelier des Etangs et al. 1993; Golimowski et al. 1993; Kalas & Jewitt 1995; Mouillet et al. 1997a, 1997b; Heap et al. 2000). These observations show various small-scale structures in the scattering disk extending from $r \sim 15$ to $\sim$1800 AU. Recent mid-infrared and submillimeter imaging observations have also overcome the contrast problem by tracing the thermal emission component from the disk because the central star is relatively faint at longer wavelengths (Lagage & Pantin 1994; Pantin et al. 1997; Wahhaj et al. 2003; Okamoto et al. 2004; Telesco et al. 2005; Holland et al. 1998). The surface brightness profile in the disk midplane changes abruptly with its radial slope at $r \sim 100$ AU. Dust grains in the disk are thought to be generated from larger bodies such as planetesimals, which resemble comets and asteroids in our solar system.

Imaging polarimetry is one of the most useful methods for studying the structure and dust properties of such extended circumstellar disks (e.g., Artymowicz 1997). However, in spite of being the most studied Vega-type stars, β Pic has rarely been the target of polarimetric observations. Gledhill et al. (1991) first performed polarimetric imaging in the *R* band with a resolution of about 1".5. Wolstencroft et al. (1995) extended the wavelengths to *B*, *V*, *R*, and *I* bands. These optical polarization data have been modeled by Voshchinnikov & Krügel (1999) and Krivova et al. (2000). The model results indicate that micron-size grains are the most important contributor to scattering and polarization of stellar radiation. To date, no near-infrared (either aperture or imaging) polarimetry studies have been reported, even though the properties of these optically dominant micron-size grains are best studied at near-infrared wavelengths.

In this paper, we present results on the AO coronagraphic imaging polarimetry of β Pic in the *K* band (2.2 μm) obtained with the 8.2 m Subaru telescope and the infrared coronagraph imager with adaptive optics (CIAO). We discuss the properties of the dust in the disk on the basis of the polarization and intensity data by employing a light-scattering dust model. Although the central $\sim$1" region is still unobservable (due to the coronagraph mask), the present data provide the first imaging polarimetry of the β Pic disk at $r = 50$–120 AU with a resolution of $\sim$4 AU, covering the possibly interesting transition zone around 100 AU.

2. OBSERVATIONS AND DATA REDUCTION

The *K*-band polarimetric imaging of β Pic was carried out on 2003 January 4, using the CIAO mounted on the Subaru Telescope (Tamura et al. 2000). The AO system was utilized under the natural seeing of 0".9 at optical wavelengths, and the FWHM of about 0".19 (=3.7 AU) was achieved in the *K*-band in spite of the large air mass (3.1–3.7) of β Pic. The pixel scale was 21.3 mas pixel^{-1} on the 1024×1024 InSb ALADDIN II array. We employed an occulting mask of 0".8 diameter. The mask was

[1] National Astronomical Observatory of Japan, Osawa, Mitaka, Tokyo 181-8588, Japan.
[2] Department of Astronomical Science, Graduate University for Advanced Studies (Sokendai), Osawa, Mitaka, Tokyo 181-8588, Japan.
[3] Department of Astrophysics, Faculty of Sciences, Nagoya University, Chikusa-ku, Nagoya 464-8602, Japan.
[4] *Spitzer* Science Center, California Institute of Technology, MC 220-6, Pasadena, CA 91125.
[5] Institute of Low Temperature Science, Hokkaido University, Sapporo 060-0819, Japan.

not completely opaque and had a transmission of ~2%, which enabled us to measure the stellar position accurately. We used a circular Lyot stop that blocked out the outer 20% of the pupil diameter.

The polarimeter consisted of a warm half-wave plate and a cold wire grid analyzer (Tamura et al. 2003). The instrumental polarization was below 1%, as measured during the commissioning of the polarimeter. The exposures were performed at four position angles (P.A.s) of the half-wave plate, in the sequence of P.A. = 0°, 45°, 22°.5, and 67°.5 to measure the Stokes I, Q, and U parameters. The integration time for each frame was 10 s (1 s × 10 co-adds), and six frames were taken before rotation of the modulator. The integration time per modulator cycle was 240 s, and six cycles of data were collected. After the imaging of β Pic, HR 1998 (A2 V) was observed as a point-spread function (PSF) reference star. The integration times for each frame and for each modulator cycle were the same as those for β Pic, and four cycles of data were collected.

The obtained frames were calibrated in the standard manner using IRAF; dark subtraction, flat-fielding by dome flats, bad pixel substitution, and sky subtraction. The sky brightness was measured as the constant mode value in the region where no emission was found in the field of view. There was no significant change of the sky during obtaining images in each cycle. The Stokes parameters (I, Q, U), the degree of polarization p, and the polarization angle θ_p were calculated as follows:

$$Q = I_0 - I_{45}, \quad U = I_{22.5} - I_{67.5},$$

$$I = (I_0 + I_{45} + I_{22.5} + I_{67.5})/2,$$

$$I_{\rm disk} = I_{\rm disk+PSF} - I_{\rm PSF},$$

$$p = \sqrt{Q^2 + U^2}/I_{\rm disk}, \text{ and}$$

$$\theta_p = (1/2)\arctan(U/Q).$$

The most dominant is the bright stellar halo, and the calculation of Q or U values corresponds to the subtraction of the unpolarized stellar PSF. Because of a temporal variation in the PSF, we rejected data that had a large intensity ratio between the central peak and the halo at $r = 1''.5$ compared with that of other data, and we checked the resultant Q and U images. We performed frame registrations using the IRAF `radprof` tool by measuring the position of the star inside the mask. We then combined images for each modulator P.A. and calculated the Q and U images for each cycle. The resultant images were binned by 9 pixels (~0".19) with the IRAF `blkavg` tool. Finally, the Q and U images were averaged over all the cycles.

The Stokes I parameter of the disk was estimated after the subtraction of the unpolarized halo of the central star. The reference PSF was obtained from the I image of HR 1998. The images of HR 1998 were registered, rotated so as to adjust the P.A.'s of the spider patterns with each other, and then combined. The PSF was subtracted after the stellar position, spider pattern direction, and the halo flux at $r = 1''.5$ of the PSF were matched to those of the I of β Pic in each modulator cycle. We checked each PSF-subtracted image and adjusted the scaling of the PSF by eye so that the halo of β Pic was satisfactory subtracted. The PSF-subtracted images of β Pic were binned by 9 pixels and the images of all modulator cycles were combined into one image. The total integration time was then 16.3 minutes for β Pic and 9.8 minutes for the PSF reference star. The reference PSF was elongated along a direction different from that of β Pic, possibly because these stars were observed at different elevations. In addition, the PSF mismatch between I_0 and I_{45}, or between $I_{22.5}$ and $I_{67.5}$, caused residuals around the masked region. Therefore, the inner region $r \leq 2''.6$ cannot be discussed. A ghost image produced by the wire grid appears at ~1".1 from the star but does not affect our results as it is located at $r < 2''.6$. Considering the uncertainty caused by the PSF subtraction (the registration, the scaling of the PSF, and the mismatch of the PSF shape), we estimated the uncertainty of $I_{\rm disk}$ as to be ~20%.

The polarization degree p was corrected with the efficiency of 97% in the K band, which was measured during the commissioning of the polarimeter. The interstellar polarization is negligible because of the proximity of β Pic, ~0.01% at optical wavelengths (Krivova et al. 2000). We calculated uncertainties in the degree of polarization by considering the standard deviations of the averages of Q and U over six cycles and the uncertainty caused by the PSF subtraction for $I_{\rm disk}$. Although we cannot estimate the consistency of each cycle because of its low signal-to-noise ratio, we confirmed the robustness of our results by calculating the polarization using only any of four cycles.

3. RESULTS

3.1. *Intensity of Circumstellar Disk*

We present the intensity image of the edge-on disk around β Pic in Figure 1. The scattered light arising from the dusty disk is detected from $r = 2''.6$ (50 AU) out to $r \sim 6''.3$ (121 AU). The outer radius is determined on the basis of the observed sensitivity, as is clear from the previous optical observations showing the outer disk of $r > 800$ AU (e.g., Smith & Terrile 1984).

Our adaptive optics observations detected the inner disk, 50 AU $< r <$ 120 AU, with a resolution of ~3.7 AU. Three observations have been reported at optical and near-infrared wavelengths, which are comparable to our results in terms of the observed inner disk and the spatial resolution (Heap et al. 2000; Mouillet et al. 1997a, 1997b). Our K-band image of the inner disk is substantially consistent with the reported images. The "warp structure" seen in these images is also confirmed in the K band.

We estimated the P.A. of the disk midplane by a least-squares fitting under the assumption that the disk has its maximum intensity along the midplane (e.g., Kalas & Jewitt 1995). The fitting was performed on the unbinned I image, and on the northeastern and southwestern wings at the same time. First, we assumed the P.A. of the midplane roughly, and we detected the pixel position on the detector if the pixel showed a maximum value in each radial step of 0".05 over the disk vertical range of 1". The linear fitting to the spatial distribution of such pixels gave the more precise P.A. of 30°.4 ± 0°.2 through the central star, measured for $r \leq 6''.0$. This value is consistent with the previous optical and near-infrared estimates for the inner disk. We adopted 30°.4 as the P.A. of the disk midplane for a comparison with a theoretical model, as described later.

Figure 2 shows the surface brightness profile measured along the disk midplane. The slope of the profile is measured by a least-squares fitting in the radial range of $2''.8 \leq r \leq 6''.0$, as $r^{-1.86\pm0.04}$ and $r^{-1.68\pm0.07}$ in the northeastern and southwestern wings, respectively. These slope values are in good agreement with those at optical wavelengths (-1.79 ± 0.01 and -1.74 ± 0.04 in the northeastern and southwestern wings, respectively, at $2''.8 \leq r \leq 6''.0$). The K'-band slopes reported by Mouillet et al. (1997a) are fitted in different radial ranges and, thus, cannot be directly compared with ours.

Note that the profile reveals a clear difference from that seen in the younger disks around pre–main-sequence stars (e.g.,

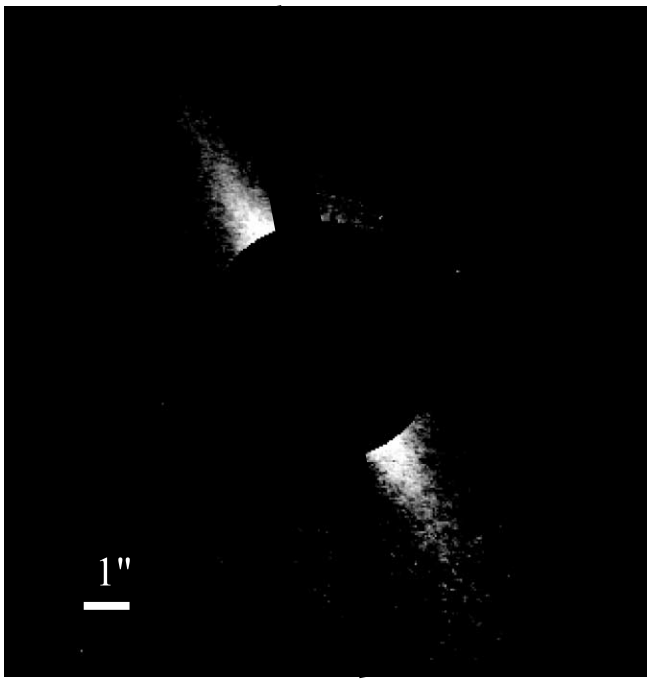

FIG. 1.—*K*-band image of edge-on disk around β Pic. The inner region ($r \leq 2\farcs6 = 50$ AU) was software masked (see text). The direction of the secondary spider pattern was also masked. The pixel scale is 21.3 mas pixel^{-1}. The image is linearly scaled and displayed from +3 to +15 σ. North is up and east is to the left.

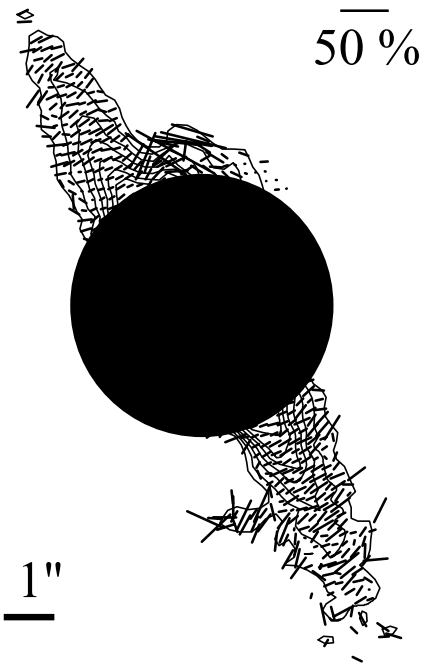

FIG. 3.—Polarization vector map in *K* band, overlaid with intensity contours. The polarization was calculated using the binned images (9 × 9 pixels); thus, the spatial scale is 0$\farcs$19. The intensity contours are created from the Stokes *I* parameter image with a raw pixel scale (0$\farcs$0213) and stars from 3 to 15 σ with a spacing of 2 σ. Note that the direction of P.A. $\sim 10^\circ$ is affected by the spider structure.

Augereau et al. 2001); the profile appears to have ripples rather than a smooth decline. We discuss the origin of the ripples in § 4.

The intensity levels in the northeastern and southwestern wings are similar at equal radii for $r \leq 6\farcs0$. This is substantially consistent with the *HST* result. We could not confirm the large ($\sim$0.5 mag) intensity asymmetry seen in the K'-band intensity profile reported by Mouillet et al. (1997a).

The vertical thickness (FWHM) of the edge-on disk was measured by fitting a Gaussian function. The fitting was applied to each radial bin of 9 pixels within a radius 80 AU where the signal-to-noise ratios are sufficiently high. Since we could not find any dependence of the FWHM on the radius, the obtained FWHMs were averaged, resulting in 18 and 19 AU in the northeastern and the southwestern disks, respectively. These FWHM values are consistent with the previous optical (15–18 AU) and near-infrared (20 AU) data.

3.2. *Polarization of Circumstellar Disk*

The *K*-band polarization map of β Pic is presented in Figure 3. The observed emission is polarized nearly perpendicular to the radial direction, indicating that grains in the disk scatter the light from the central star. Although there are some regions where vectors deviate from the centrosymmetric pattern, they are confined to regions where the signal-to-noise ratios are relatively poor. Thus, the β Pic disk is seen as an infrared reflection nebula as in the

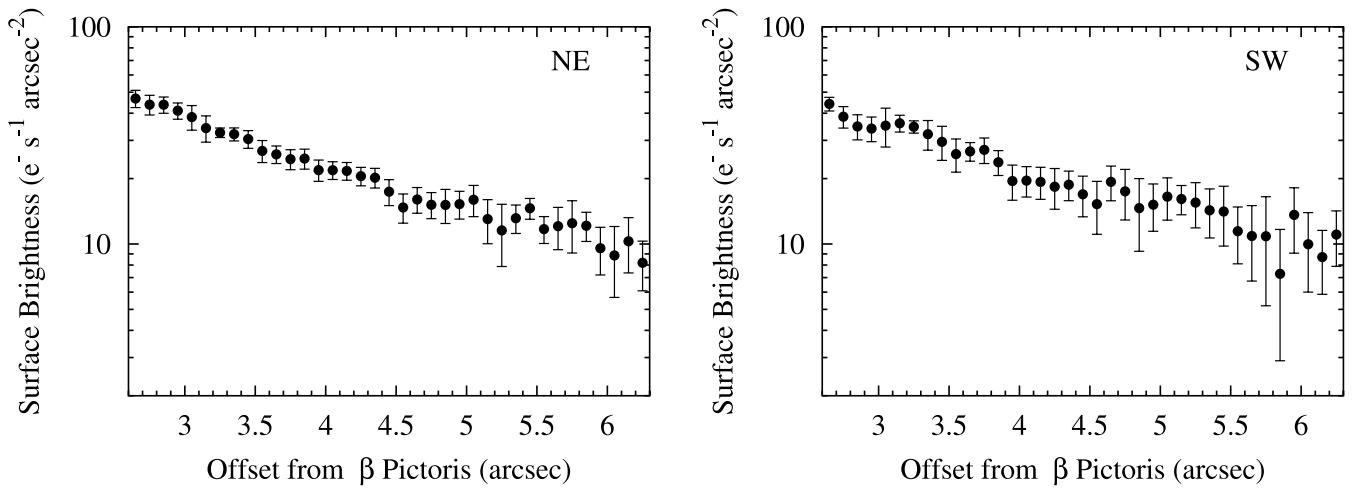

FIG. 2.—Surface brightness distribution along disk midplane for northeastern disk (*left*) and southwestern disk (*right*). The surface brightness was averaged over the disk vertical thickness of 0$\farcs$19 and the radial range of 0$\farcs$1.

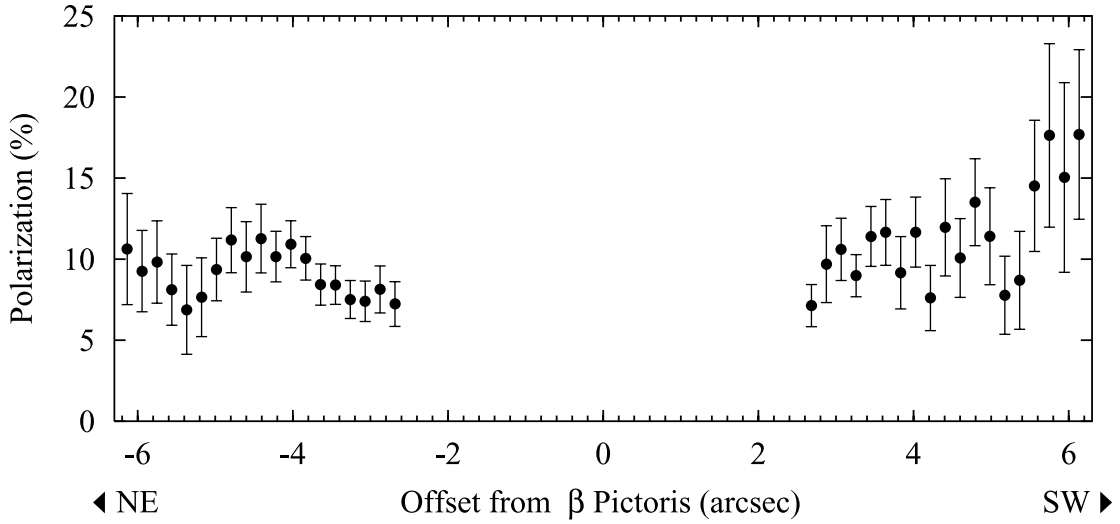

FIG. 4.—Degree of polarization in *K* band measured along disk midplane.

case at optical wavelengths (Gledhill et al. 1991; Wolstencroft et al. 1995).

We show the *K*-band degree of polarization along the disk midplane in Figure 4. We detected about 10% polarization in 50 AU $< r <$ 120 AU. The degrees of polarization are roughly the same for the northeastern and southwestern wings, as for the radial surface brightness levels. In contrast, the optical polarization data show a substantially higher level of polarization ($\sim$15% at $r >$ 150 AU) and a higher polarization with an asymmetrical distribution in the southwestern wing. Since the uncertainty is large in the outer southwestern wing ($r >$ 100 AU), we cannot claim that the polarization increases with radius. Note that there is a dip in the polarization levels around $r \sim$ 100 AU in both wings.

3.3. *Model*

In this section, we compare the results of our polarization measurements with detailed model calculations to gain an insight into the properties of dust grains in the debris disk around β Pic. We code for model polarized intensities by incorporating Mie theory into the algorithm that is described in Artymowicz et al. (1989). Numerical calculations require reasonable assumptions concerning the spatial and size distribution of dust grains (Artymowicz et al. 1989; Artymowicz 1997). Krivova et al. (2000) have successfully reproduced the dependences of linear polarization on wavelength and radial distance by assuming the presence of homogeneous spherical silicate grains throughout the disk. We calculated the Stokes parameters (I, Q, U) using Mie theory and subsequently the degree of linear polarization $P = (Q^2 + U^2)^{1/2}/I$ by employing their model parameters: The disk is inclined by 4° with respect to the line of sight and truncated at $r = 1000$ AU in cylindrical coordinates (r, z), the radius of dust grains ranges from $a_{\min} = 5$ nm to $a_{\max} = 100$ μm, and the spatial and size distribution $n(r, z, a)\, da$ in the range of dust radius from a to $a + da$ is described as

$$n(r,\ z,\ a) = n_0 \exp\left\{-\left[\frac{|z|/r_0}{0.05(r/r_0)^{\eta}}\right]^{1.1}\right\} \times \left[\left(\frac{r}{r_0}\right)^{-1} + \left(\frac{r}{r_0}\right)^{2.7}\right]^{-1} a^{-3.5}, \quad (1)$$

where $r_0 = 116$ AU (i.e., 6″) and $\eta = 1.2$, as used for the outer disk model of Krivova et al. (2000). In the inner disk at distances of $r \le r_0$, however, we set $\eta = 0$, as inferred from our near-infrared measurements of the inner disk. Stellar radiation pressure reduces the number density of grains with $a \le a_0$ by blowing them out of the system. Here a_0 is the dust radius at which the ratio of radiation pressure to stellar gravity reaches 0.5 (see, e.g., Zook & Berg 1975). Note that once the composition of grains is assumed, the "blown-out" radius a_0 and the amount of the reduction in the number density are no longer

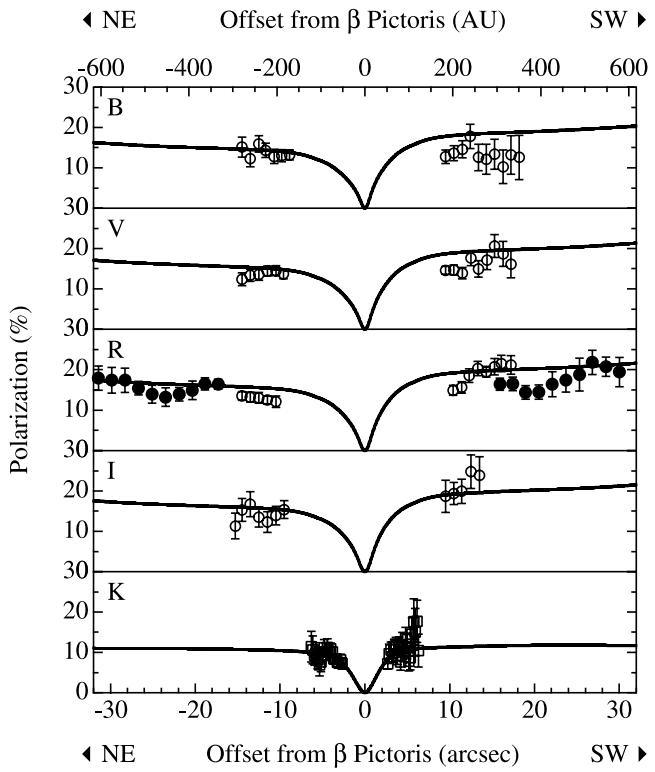

FIG. 5.—Linear polarization as a function of offset from β Pic. *Solid curves*: Our model results; *squares*: our *K*-band data; *filled circles*: *R*-band data from Gledhill et al. (1991); *open circles*: *B*-, *V*-, *R*-, and *I*-band data from Wolstencroft et al. (1995).

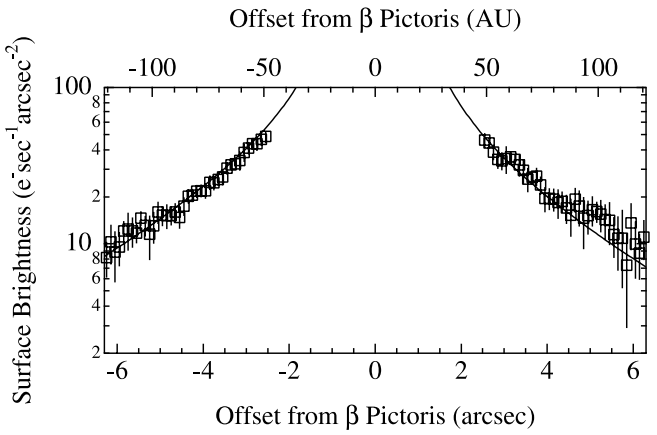

FIG. 6.—*K*-band intensity as a function of offset from β Pic. *Solid curves:* Our model results; *squares:* our *K*-band data.

free parameters. We take the refractive indices of "astronomical silicate" from Laor & Draine (1993), for which $a_0 = 2.0$ μm (see Kimura & Mann 1999). An estimate of the reduction factor for the density n_0 is not trivial, because a nonlinear equation along with assumptions for unknown sources of dust has to be solved (Krivov et al. 2000). Here we simply reduce the number density for dust grains having radius $a \leq a_0$ by a factor of 10 in the northeastern wing of the disk and by 15 in the southwestern wing. We note that our observed *K*-band polarization turned out to be inconsistent with the reduction factors of approximately 15 (northeastern) and 20 (southwestern) adopted by Krivova et al. (2000).

Figure 5 shows the model polarization in the midplane (*solid curves*) plotted together with our near-infrared data (*open squares with error bars*) as well as currently available optical data from Gledhill et al. (1991; *filled circles with error bars*) and Wolstencroft et al. (1995; *open circles with error bars*). Prior to calculations of the polarization, the derived Stokes parameters were integrated over 1″ both optical and infrared data in a direction perpendicular to the midplane. Note that the model properly reproduces the absolute values and spectral variation of the linear polarization, as well as its northeast-southwest asymmetry at optical wavelengths and northeast-southwest symmetry at near-infrared wavelengths. We also found that the radial profile of the observed *K*-band intensity agrees with our numerical results for the Stokes *I* parameter (Fig. 6). Our numerical simulations in the optical wavelength range provide a neutral color in the outer disk, consistent with the multiple-wavelength data from Paresce & Burrows (1987) and Lecavelier des Etangs et al. (1993). The color becomes slightly redder in the inner part of the disk, but we cannot reconcile the strong decrease in the *B*-band brightness that was observed by Lecavelier des Etangs et al. (1993).

4. DISCUSSION

The observed *K*-band polarization is characterized by its low value and northeast-southwest symmetry, in contrast to the high value and asymmetrical distribution of the optical polarization. To better understand this wavelength dependence, we consider the blown-out radius in comparison with the radius of dust particles that mainly determines the degree of linear polarization at each wavelength of the observations. It is worth noting that dust grains in the Rayleigh scattering regime ($a \ll \lambda$) as well as in the geometrical optics regime ($a \gg \lambda$) produce a polarization much higher than that observed, while grains in the Mie scattering regime ($a \approx \lambda$) lower the polarization (Voshchinnikov & Krügel 1999). At optical wavelengths, Mie scattering particles are smaller than the blown-out radius (i.e., $a < a_0$) and therefore their abundances are lowered. As a result, the optical polarization is kept high, in particular, in the southwestern wing, where the number of Mie scattering particles is greatly reduced. Provided that the radius of Mie scattering particles is comparable to or larger than the blown-out radius (i.e., $a \gtrsim a_0$), the polarization becomes low and symmetrically distributed. The low and northeast-southwest symmetrically distributed polarization observed in the *K*-band implies that the blown-out radius a_0 lies in the range of microns, consistent with $a_0 = 2$ μm in our model.

The model uses compact, spherical, optically bright silicate grains whose properties are in accord with the high albedo estimated by Backman et al. (1992). Optically bright compact grains are consistent with the blown-out radius of a few microns necessary for explaining the observed low *K*-band polarization. Regardless of our successful results, however, spherical silicate grains are not necessarily representative of real dust particles in the β Pic debris disk. Mid-infrared spectroscopic observations have revealed a similarity between dust in the β Pic debris disk and cometary dust in the solar system (Knacke et al. 1993). Cometary dust is likely an optically dark fluffy aggregate consisting of submicron-sized grains (Greenberg & Gustafson 1981; Kimura et al. 2003). In a model with dust aggregates for the β Pic system, a problem is encountered in that the blown-out radius of fluffy aggregates is much larger than a few microns (cf. Kimura & Mann 1999). To resolve this apparent discrepancy, we here consider icy parent bodies "planetesimals" that consist of ice and dust, analogous to cometary nuclei in the solar system (see Yamamoto 1985). After ejection from their parent bodies, dust particles are still encased in ice at the distances of our observations, although we have to keep in mind the possibility that the intense ultraviolet radiation from β Pic erodes icy grains by photo sputtering (see Artymowicz 1994). If ice fills the pores of optically dark dust aggregates, then the dust may resemble optically bright compact particles. The refractive indices of ice with optically dark inclusions are close to those of silicates, depending on the volume fraction of the inclusions (see Mukai et al. 1986). As a result, the blown-out radius of ice-filled, optically dark aggregates would lie in the range of microns, as expected for dirty water-ice spheres (cf. Artymowicz 1988). Our results may indicate that compact spherical silicate grains are simply a good approximation for ice-filled fluffy aggregates of optically dark submicron grains existing in the β Pic system.

Although the smooth model curves fit the intensity and linear polarization profiles in the *K* band well, a noticeable dip appears in both the intensity and polarization profiles at 5.″2–5.″4 (i.e., 102–104 AU) along both directions (Figs. 2 and 4), except for in the southwestern intensity profile. The dip is also seen in the *pI* profile, indicating that it is not caused by an artifact due to the PSF subtraction for $I_{\rm disk}$. We here interpret the dip in terms of a gap in the radial density distribution of dust grains around 100 AU from the central star. Keeping in mind that the observed radiation is an integrated quantity over a line of sight, the effect of a gap on the integrated quantity depends on its integrand. By analogy to interplanetary dust or cometary dust, we expect the integrand of intensity to show a strong forward scattering enhancement and the integrand of polarization to peak around a scattering angle of 90° (Artymowicz 1997). Although a deficit of dust grains reduces the intensity, forward scatterers residing far from the gap region tend to obscure the reduction. This may explain why the dip in the intensity profile is seen only on the northeast side of the disk, where the signal-to-noise ratio is

higher than the southwest side. When the line of sight is tangent to a gap in the radial dust density, a low degree of polarization results from a lack of dust grains having scattering angles around 90°. On the other hand, an erroneous hump in the intensity profile would decrease the polarization, but simultaneous decreases in both the intensity and the polarization do not seem to be coincidental. Mouillet et al. (1997a) measured the *K*-band surface brightness of the β Pic disk, in which we confirm the presence of a similar dip around 5.″2. It is highly unlikely that both we and Mouillet et al. (1997a) erroneously obtained a dip at the same distance from the star on the basis of independent data and analyses. Therefore, this dip is not an artifact arising from our data analysis, but is a real signature corresponding to the depletion of dust grains around 100 AU. We expect that dust grains are located near their parent-body planetesimals, because grains are destroyed by mutual collisions before being transported inward by the Poynting-Robertson effect in the β Pic system (Artymowicz 1997; Krivov et al. 2000). Consequently, the dip in the intensity and polarization profiles around 100 AU is evidence for a paucity of planetesimals in this region.

Our *K*-band intensity data reveal not only the dip around 100 AU but also ripple structures over the entire observed disk region between 50 and 121 AU (see Fig. 2). Comparing our intensity data with the results of Mouillet et al. (1997a), we realize that there is a great similarity between the ripple structures obtained in the two independent observations. If all the humps in the ripple structures are in fact planetesimal belts, then our data indicate that the β Pic disk consists of multiple planetesimal belts. Several planetesimal belts (rings) have already been identified from mid-infrared observations of the β Pic disk in the inner region ($r < 90$ AU) (Wahhaj et al. 2003; Okamoto et al. 2004; Telesco et al. 2005). Recent observations have revealed that the β Pic debris disk resembles the circumstellar disk around AU Microscopii, including spatially localized enhancements and deficits (Liu 2004; Metchev et al. 2005). Therefore, we conclude that the presence of multiple planetesimal belts is common in circumstellar disks around Vega-type stars.

M. T., H. K., and T. Y. are supported by Grants-in-Aid from the Ministry of Education, Culture, Sports, Science, and Technology. M. F. is supported by the JSPS Research Fellowships for Young Scientists.

REFERENCES

Artymowicz, P. 1988, ApJ, 335, L79
———. 1994, in Circumstellar Dust Disks and Planet Formation, ed. R. Ferlet & A. Vidal-Madjar (Singapore: Editions Frontieres), 47
———. 1997, Annu. Rev. Earth Planet. Sci., 25, 175
Artymowicz, P., Burrows, C., & Paresce, F. 1989, ApJ, 337, 494
Augereau, J. C., Lagrange, A. M., Mouillet, D., & Ménard, F. 2001, A&A, 365, 78
Aumann, H. H., et al. 1984, ApJ, 278, L23
Backman, D. E., Gillett, F. C., & Witteborn, F. C. 1992, ApJ, 385, 670
Barrado y Navascués, D., Stauffer, J. R., Song, I., & Caillaut, J.-P. 1999, ApJ, 520, L123
Crifo, F., Vidal-Madjar, A., Lallement, R., Ferlet, R., & Gerbaldi, M. 1997, A&A, 320, L29
Gledhill, T. M., Scarrott, S. M., & Wolstencroft, R. D. 1991, MNRAS, 252, 50P
Golimowski, D. A., Durrance, S. T., & Clampin, M. 1993, ApJ, 411, L41
Greenberg, J. M., & Gustafson, B. Å. S. 1981, A&A, 93, 35
Heap, S. R., et al. 2000, ApJ, 539, 435
Holland, W. S., et al. 1998, Nature, 392, 788
Kalas, P., & Jewitt, D. 1995, AJ, 110, 794
Kimura, H., Kolokolova, L., & Mann, I. 2003, A&A, 407, L5
Kimura, H., & Mann, I. 1999, Phys. Chem. Earth C, 24, 561
Knacke, R. F., Fajardo-Acosta, S. B., Telesco, C. M., Hackwell, J. A., Lynch, D. K., & Russell, R. W. 1993, ApJ, 418, 440
Krivov, A. V., Mann, I., & Krivova, N. A. 2000, A&A, 362, 1127
Krivova, N. A., Krivov, A. V., & Mann, I. 2000, ApJ, 539, 424
Lagage, P. O., & Pantin, E. 1994, Nature, 369, 628
Laor, A., & Draine, B. T. 1993, ApJ, 402, 441
Lecavelier des Etangs, A., et al. 1993, A&A, 274, 877
Liu, M. C. 2004, Science, 305, 1442
Metchev, S. A., Eisner, J. A., Hillenbrand, L. A., & Wolf, S. 2005, ApJ, 622, 451
Mouillet, D., Lagrange, A. M., Beuzit, J.-L., & Renaud, N. 1997a, A&A, 324, 1083
Mouillet, D., Larwood, J. D., Papaloizou, J. C. B., & Lagrange, A. M. 1997b, MNRAS, 292, 896
Mukai, T., Fechtig, H., Grün, E., Giese, R. H., & Mukai, S. 1986, A&A, 167, 364
Okamoto, Y. K., et al. 2004, Nature, 431, 660
Pantin, E., Lagage, P. O., & Artymowicz, P. 1997, A&A, 327, 1123
Paresce, F., & Burrows, C. 1987, ApJ, 319, L23
Smith, B. A., & Terrile, R. J. 1984, Science, 226, 1421
Tamura, M., Fukagawa, M., Murakawa, K., Suto, H., Itoh, Y., & Doi, Y. 2003, Proc. SPIE, 4843, 190
Tamura, M., et al. 2000, Proc. SPIE, 4008, 1153
Telesco, C. M., et al. 2005, Nature, 433, 133
Voshchinnikov, N. V., & Krügel, E. 1999, A&A, 352, 508
Wahhaj, Z., Koerner, D. W., Ressler, M. E., Werner, M. W., Backman, D. E., & Sargent, A. I. 2003, ApJ, 584, L27
Wolstencroft, R. D., Scarrott, S. M., & Gledhill, T. M. 1995, Ap&SS, 224, 395
Yamamoto, T. 1985, A&A, 142, 31
Zook, H. A., & Berg, O. E. 1975, Planet. Space Sci., 23, 183